The Formation of Natural Gypsum Megacrystals in Naica (Mexico)

Supplementary Information deposited into the GSA Data Repository.

Juan Manuel García-Ruiz[1], Roberto Villasuso[2], Carles Ayora3, Angels Canals[4], Fermín Otálora[1]

[1] Instituto Andaluz de Ciencias de la Tierra. Consejo Superior de Investigaciones Científicas-Universidad de Granada, Campus Fuentenueva, E-18002, Granada, Spain
[2] Compañía Peñoles, Unidad Naica, Naica, Chihuahua, Mexico.
[3] Institut de Ciències de la Terra Jaume Almera, Consejo Superior de Investigaciones Científicas, Lluis Solé Sabarís s/n, E-08028 Barcelona, Spain
[4] Dept. de Cristal·lografia, Mineralogia i Dipòsits Minerals, Universitat de Barcelona, Martí Franquès s/n, E-08028 Barcelona, Spain

1. Supplementary Figures and legends

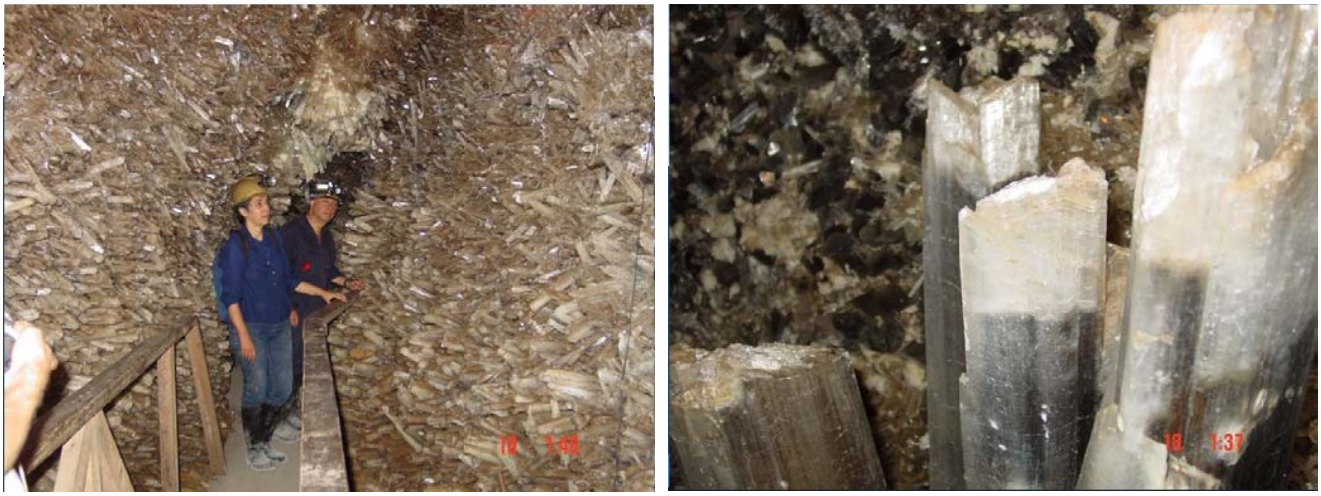

Figure DR1: *The Cueva de las Espadas* (Cave of the Swords) discovered in 1910 is located at level −120 m close to the Montaña fault (see Fig. 1). It is a long corridor (shown on the left) which walls are entirely covered by crystals from centimeter to almost a meter in size (Degoutin, 1912; Foshag, 1927). The cave is close to the natural phreatic level and this explains the light grey and black color of the crystals due to clay as well as iron and manganese oxides solid inclusions (right). These solid inclusions are in most cases aligned on growth fronts, suggesting the occurrence of episodic avalanches of strong oxidation and a growing environment from muddy waters containing colloidal clays.

2. Supplementary methods

2.1. Gypsum Crystal Habit

The habit of gypsum crystals from the Cave of the Crystals has been studied by single crystal X-ray diffraction and by laser reflection goniometry. X-ray diffraction experiments on cleavage plates were performed to get the first inputs on crystal orientation and morphology as well as the unit cell parameters required for the geometrical calculations of inter-facial and inter-edge angles. Our laboratory diffractometer, a Bruker Proteum X8 equipped with a Microstar generator, and a KappaCCD goniometer and detector was used for these X-ray diffraction studies. The unit cell parameters of the crystals investigated were a=5.684Å, b=15.189Å, c=6.282Å, β=114.10º; the face parallel to the main cleavage is, as expected, {0 1 0} and the elongation of the crystals was identified to be [0 0 1].

Interfacial angles (Fig. DR2b) were measured using a straight edge and a protractor for macroscopic forms and a simple light goniometer for microscopic faces (Fig. DR3). These studies indicate that the crystals are prisms bounded by {0 1 0} and {1 k 0} faces and caped by {-1 1 1} faces (Fig. DR2a). The {1 k 0} faces are striated and composed of alternating bundles of {1 2 0}, {1 4 0} and {1 6 0} faces making and overall orientation close to {1 4 0} (Fig. DR4 and table DR1).

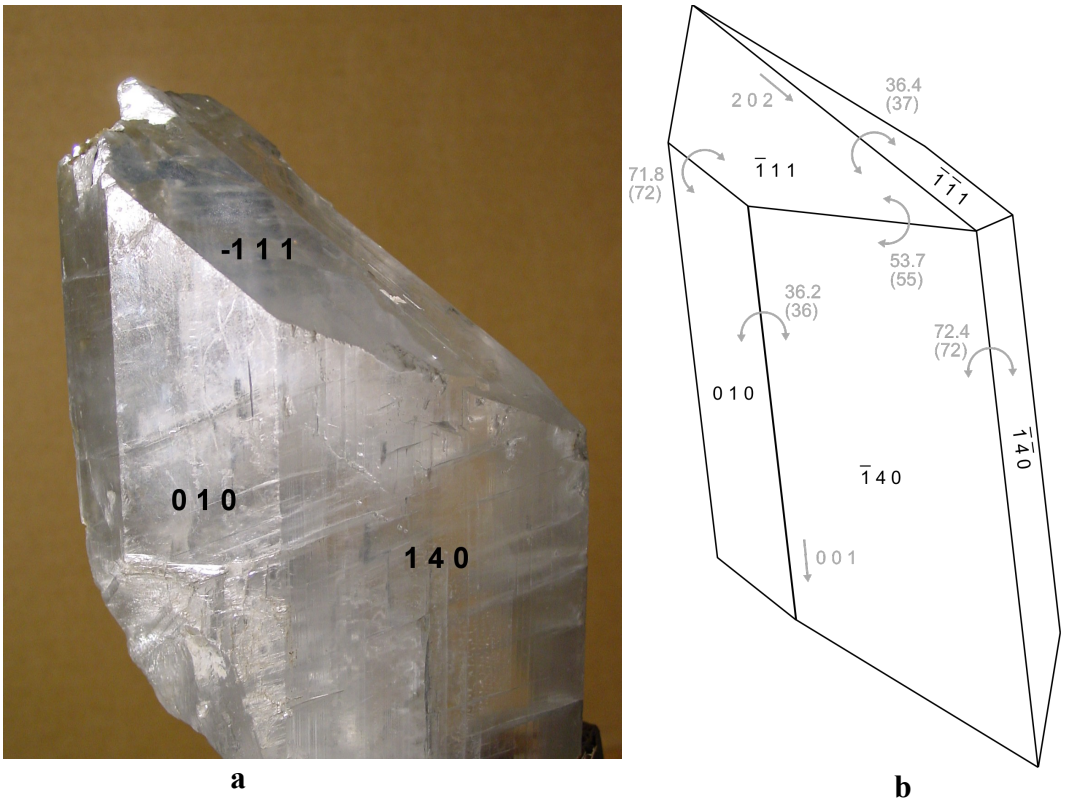

Figure DR2: a) Large blocky gypsum crystal from the *Cueva de los Cristales*. The crystal size in the vertical direction is 12 cm. b) Sketch of the crystal habit showing the indices of the faces, the main zone directions (arrows) and the main interfacial angles (curved double arrows). The numbers next to the double arrows show the values computed from the unit cell followed by the measured angles in parentheses.

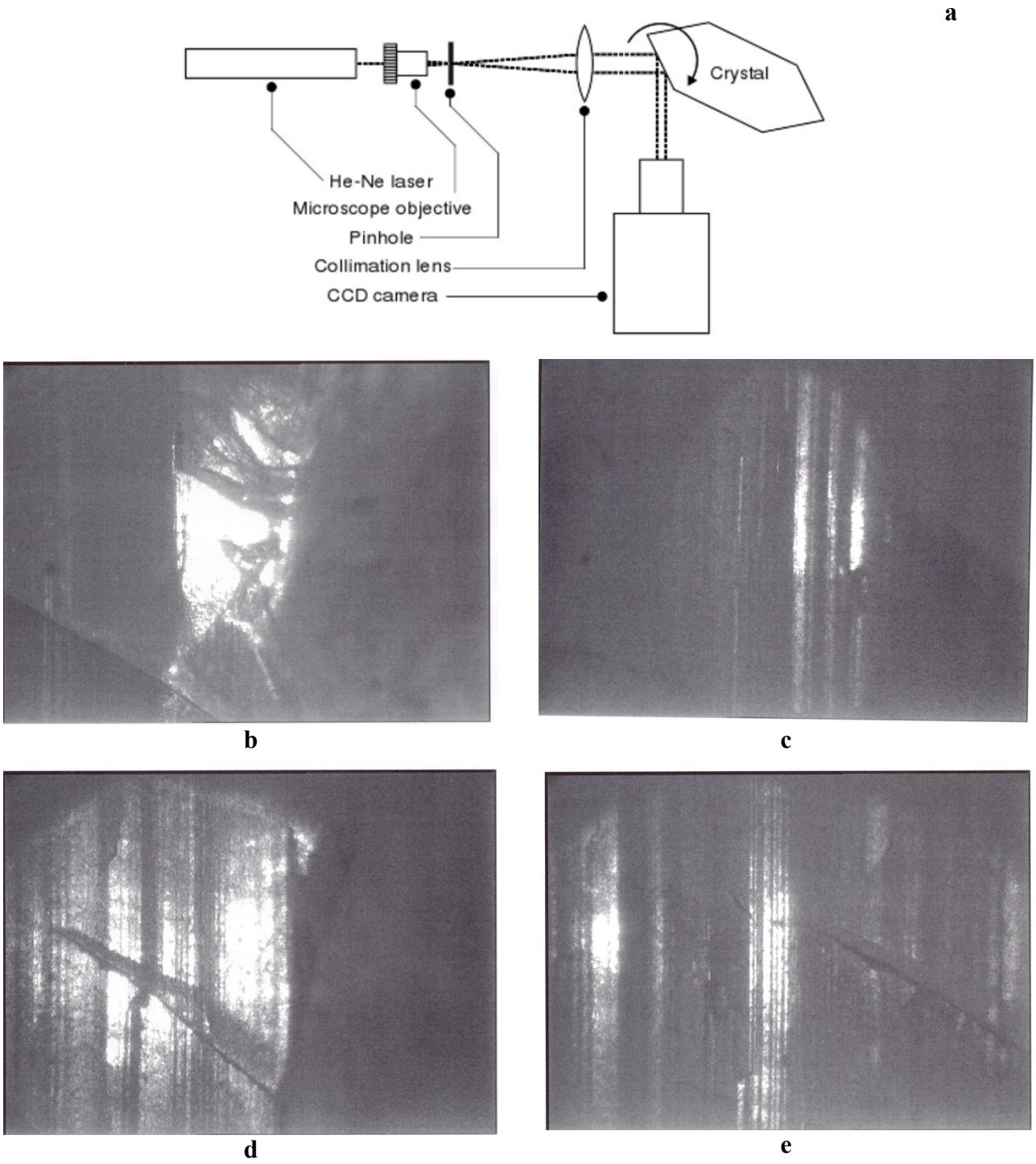

Figure DR3: a) Experimental setup of the laser goniometer used for the measurement of angles between mirror reflections belonging to the [001] zone. b) Reflection on the (0 1 0) face as seen from the CCD camera. c-e) Mirror reflections from, respectively, (1 2 0), (1 4 0) and (1 6 0). The angles at which these pictures were collected are shown in Table DR1 (third column)

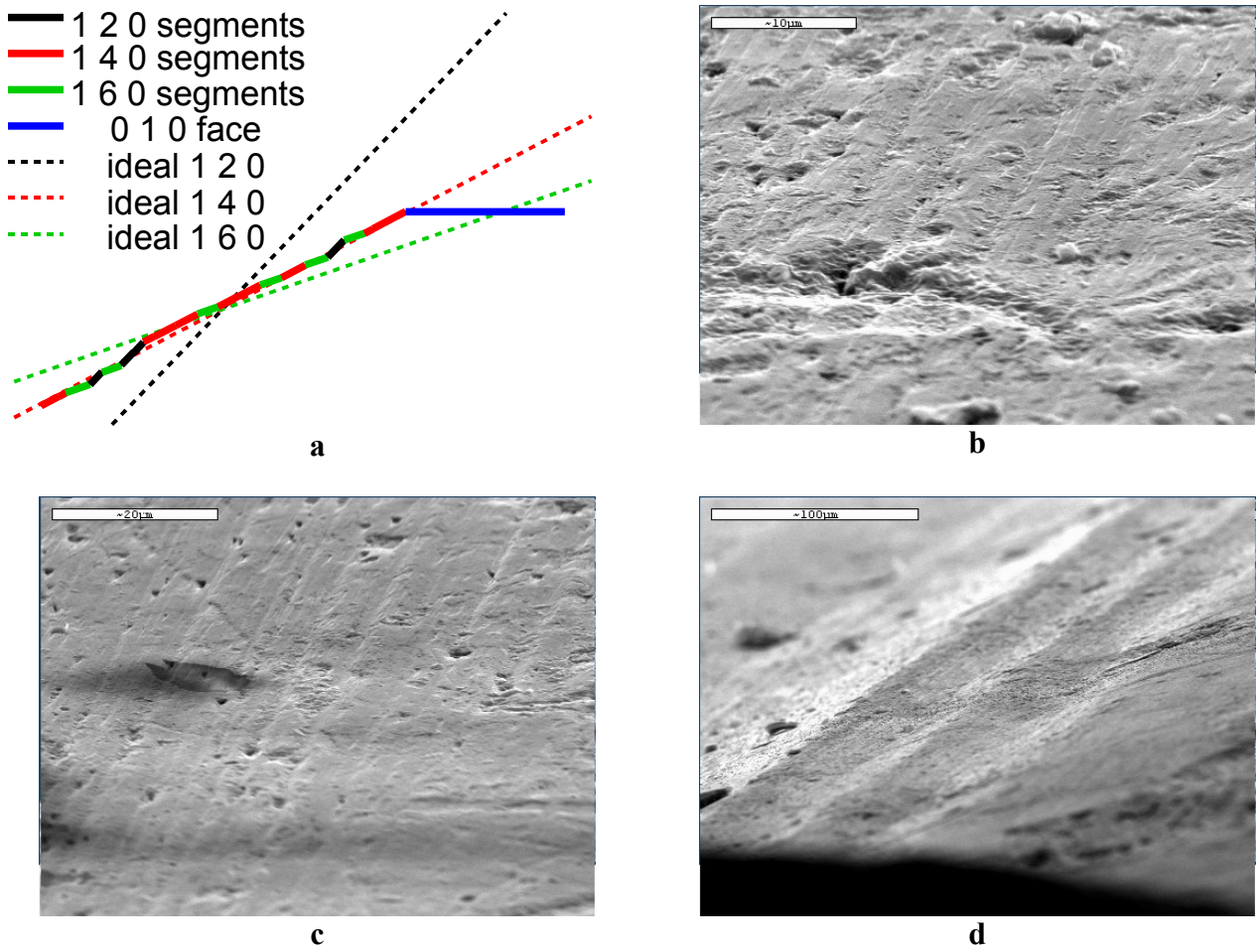

Figure DR4. Structure of the {1k0} surface. a) Sketch of the face segments distribution and the corresponding angles. b-d) Scanning electron microscope views of the surface showing the variable face segments at three different magnifications..

Table DR1: Calculated and measured angles between 010 and 1k0. The measured angles can be assigned to k = 2, 4, 6

Face	Angle (calculated)	Angle (measured)
010	0.00	0
110	71.14	-
120	55.66	51
130	44.30	-
140	36.20	34
150	30.35	-
160	26.01	25
170	22.69	-

Figure DR5: Top view of a crystal beam showing the terminal faces {-111}: Notice that the large development of the prism {1k0} provokes very small pinacoidal {010} faces.

Figure DR6: Two examples of blocky crystals. The unusual blocky habit, the development of the more acute prismatic faces {140} and {160} instead of the usual {120} (Simon and Bienfait, 1965) and the alignment of the crystals with the edge [010] vertical, give them a distinctive sharktooth appearance.

2.2. Fluid inclusions

Fluid inclusion petrography and microthermometry were performed in less than 0,1m long gypsum cleavage fragment from a gypsum sample of the Cave of Crystals, where clear primary fluid inclusions related to growth bands were observed. The large fragment of the crystal from Cave of the Crystals was first sawed using an oil saw. Inclusions sizes range from 40 to 600μm and most of them display a idiomorphic shape. Microthermometry of fluid inclusions was carried out on a Linkam THMS 600 heating and freezing stage. All measurements were made using a 10× objective lens. Calibration of the stage was checked using pure CO_2 and H_2O inclusions. Although heating rates seem not to have a crucial role for regular fluid inclusions microthermometric results, as we work with large inclusions and thick gypsum slices we checked different heating rates and fragment sizes. We concluded that in our case the heating rate must be as slow as 0.1 ºC/minute near the final melting temperature, and the slices must be thinner than 1mm.

Primary fluid inclusions from gypsum growth bands were in most cases monophasic (liquid phase) at room temperature (Figure DR7). Less than 5% of them, however, also show a gas bubble. This suggests that inclusions were formed from a liquid phase at higher temperatures, but the gas phase bubble did not usually nucleate because the temperature gap to the room temperature is short. In order to increase the cooling interval, gypsum fragments were located and maintained at 2 ºC for few weeks and as expected, about 15% of inclusions showed a gas bubble after the cooling. Only those inclusions which were biphasic at room temperature were selected for cryogenic studies (33 fluid inclusions). Eutectic temperatures were not clearly observed in any run. Melting ice temperatures show a maximum at -0.1 with a dispersion of the values down to -1.1 ºC (Fig. DR10). This range of temperatures indicates a low salinity conventionally expressed in the NaCl-H_2O system: 0.17 mass % NaCl with values increasing up to 1.9 mass % NaCl (Bodnar, 1993; Bakker, 2003). The dispersion of melting ice temperatures within an inclusion band is of the same order of magnitude of the variations along the whole set of samples and, therefore, no significant salinity variation with crystal growth can be established.

Heating experiments were performed in 31 fluid inclusions which were biphasic at room temperature. To avoid possible damage, the crystal fragments used in freezing experiments were discarded for heating. Homogenization took place to liquid phase, at temperatures showing a normal distribution with a maximum around 54±7 ºC (Table DR2). From the geological setting no correction due to confinement pressure is required, so this temperature range can be considered the actual temperature of crystal growth.

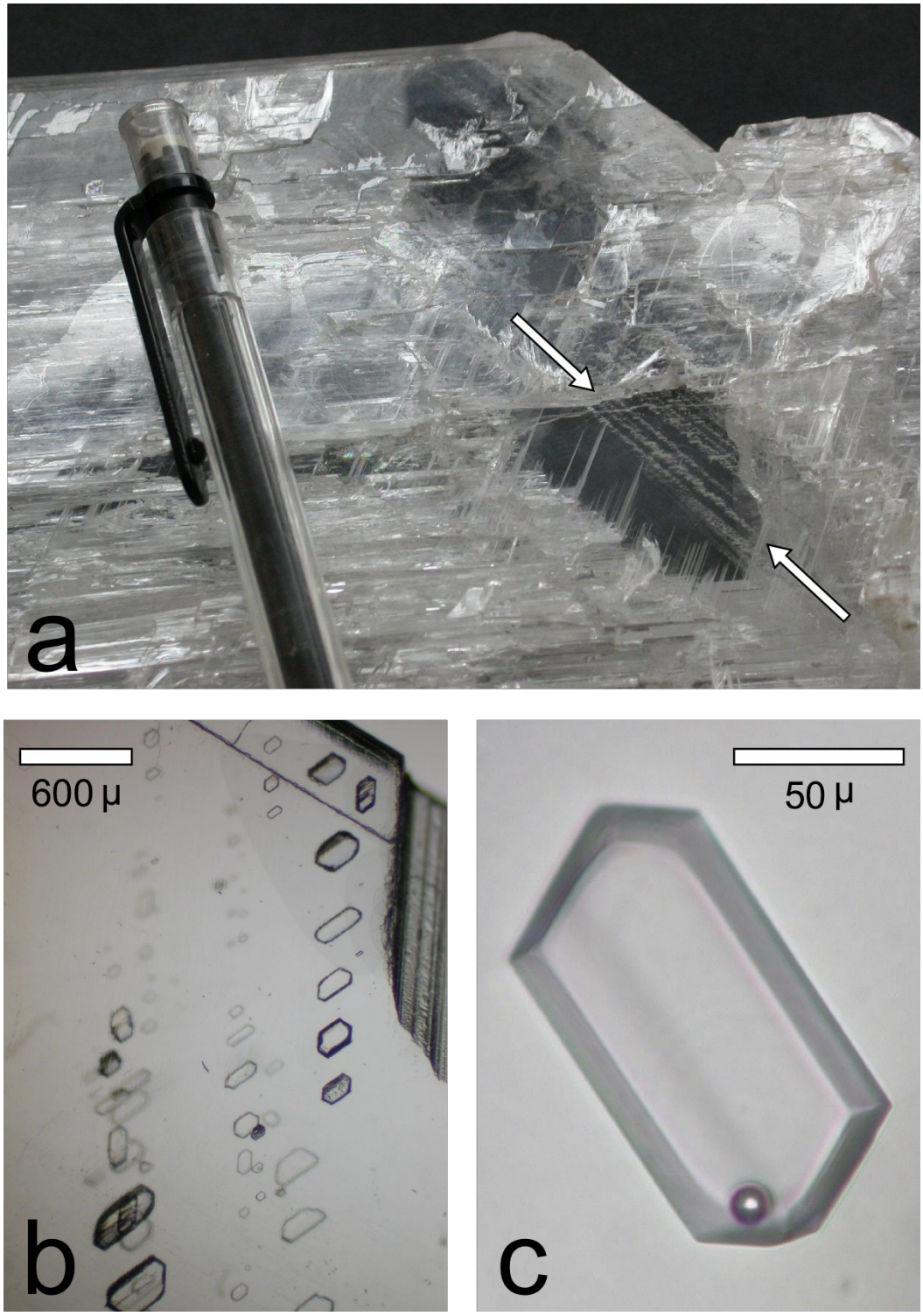

Figure DR7: a) Gypsum crystal form the Cave of Crystals showing growth bands with primary fluid inclusions (arrows). b) A detail of these inclusions along growth fronts. c) Detailed view of one of the biphasic inclusions used in the study.

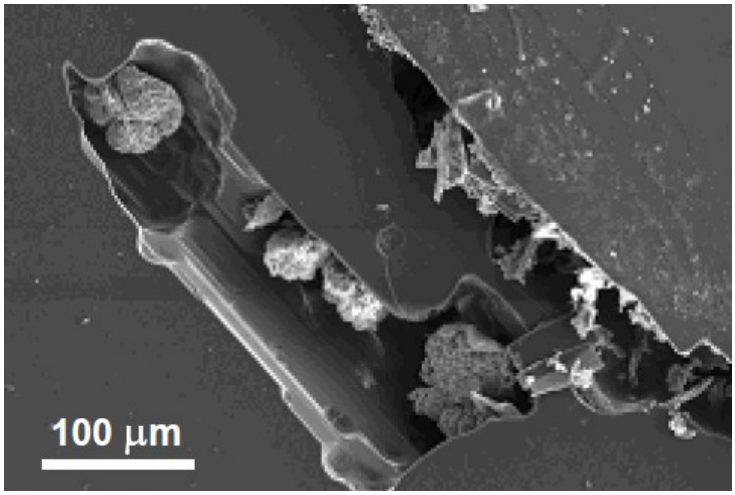

Figure DR8: Spherulitic solid inclusions trapped within fluid inclusions in gypsum crystals from the Cave of Crystals.

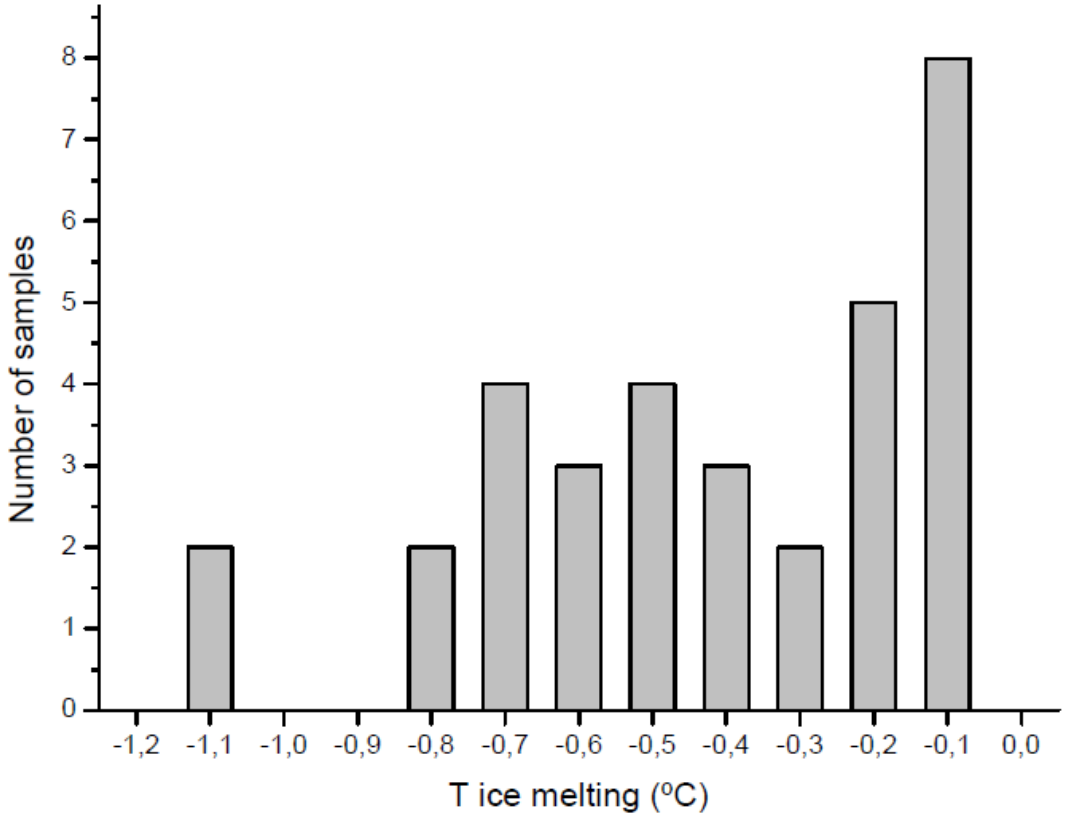

Figure DR9: a) Ice melting temperatures from 33 selected fluid inclusions which were biphasic at room temperature. The range of obtained temperatures (-0.1 ºC to -1.1 ºC, with a maximum at -0.1 ºC) indicates a low salinity of 0.31 mass % NaCl (for -0.1 ºC) up to 1.9 mass % NaCl (for -1.1 ºC).

Table DR2: Measured values of the homogenisation temperatures

54,1	53,5	54,3	50,5	52,6	52,1	54,5	54,5
54,0	52,7	48,3	56,4	60,0	58,3	61,5	57,8
52,0	52,0	51,4	46,7	46,0	46,0	38,1	49,1
51,6	56,2	54,2	52,3	53,6	56,2	48,1	

Solid inclusions have a spherulitic texture and are located within the fluid inclusions (Fig. DR8). The spherulites have a black core and a red halo under transmitted light microscopy, and SEM-EDS microanalysis shown that they are made of Mn, Fe, and Pb, and minor amounts of Si, Al, Na, Zn, and Cu. No X-ray diffraction pattern could be obtained from this spherulitic material. Similar spherulites are found in abundance in the Cave of Swords, where they produce the dark grey color of the gypsum crystals. The XRD pattern of this material shows two peaks (4.91 Å and 2.95 Å) corresponding to Mn_5O_8 compound (J17-0962 card).

2.3. Isotopic analysis

Several samples of anhydrite and gypsum from different locations in the mine were collected for stable isotope analysis. A representative sample of 0.1g of the mineral was first dissolved in 50mL of miliQ water. The dissolved sulfate was then precipitated as $BaSO_4$ by the addition of $BaCl_2{\cdot}2H_2O$ in acidic media (pH<2) to prevent $BaCO_3$ precipitation. The $\delta^{34}S$ was determined from $BaSO_4$ with an elemental analyzer coupled in continuous flow with a δC mass spectrometer. The $\delta^{18}O$ was measured in duplicate by on-line pyrolisis coupled with a δC mass spectrometer. The data were reported in the usual $\delta^{34}S$ CDT notation for the sulfur, and $\delta^{18}O$ SMOW for the oxygen. The overall reproducibility for the samples and laboratory internal standards was better than ±0.2‰ for sulfur and ±0.5‰ for oxygen.

The sulfur and oxygen isotopic composition of 17 sulfates (eight gypsum crystals, eight anhydrite crystals and one from water collected at level 530 are shown in Table DR3. Two $\delta^{34}S$ and $\delta^{18}O$ values of gypsum from Cave of the Crystals show no variation, besides the habit of the crystals (beams or blocky), with a $\delta^{34}S$ of 16.9‰ and the $\delta^{18}O$ of 17.6‰. One sample from the Cave of the Queen (sample 22) and another collected close to the Cave of the Crystals (sample 28) have similar isotopic composition. Gypsum samples from the Cave of the Swords (level 120) have slightly lower $\delta^{18}O$ values, 1‰ less than samples from the Caves of the Crystals and the Queen (level 290). The isotopic composition of the mineralizing solution is estimated to be around $\delta^{34}S$=15.3±0.2‰, with a gypsum-solution enrichment factor of 1.65‰ (value at 25°C) for sulfur (Thode and Monster, 1965), and $\delta^{18}O$=14.3‰, for a gypsum-solution enrichment factor of 3.3‰ (value at 55°C) for oxygen (Pearson and Rightmire, 1980). These values are perfectly consistent with the isotope composition of the present day water collected at level 530 (Fig. 3 and Table DR3). As seen in the same figure, the isotopic values of sulfate dissolved in the water could be explained by mixture of sulfates from the dissolution of anhydrite from different locations of the mine, those from the ore deposit area (samples 23, 24, 25 and 34) and those from upper levels in the mine (samples 4 and 21).

Table DR3: Isotopic composition of Naica samples.

sample	Mineral	location	$\delta^{34}S$	$\delta^{18}O$
9	Gyp.	Cave of the Swords	17,3	16,5
8	Gyp.	Cave of the Swords	17,6	16,7
15	Gyp.(beam)	Cave of the Crystals	17	17,4
31	Gyp.(blocky)	Cave of the Crystals	16,8	17,8
4	Anh.	close to Cave of the Crystals	16	13,7
28	Gyp.	close to Cave of the Crystals	16,3	17,8
21	Anh.	Cave of the Queen	16,7	13,0
22	Gyp.	Cave of the Queen	16,8	17,7
23a	Anh.	Ore body	14,4	16,0
24a	Anh.	Ore body	14,9	15,6
25a	Anh.	Ore body	13,8	15,7
25b	Gyp.	Ore body	17	17,9
34a	Anh.	Ore body	12,9	14,3
34b	Gyp.	Ore body	16,5	17,0
35	Anh.	level 590	13,8	14,7
36	Anh.	level 700	14,6	15,6
26	Water	level 530	14,6	14,4

2.4. Hydrochemistry

Two samples of groundwater from the levels 640 and 530 have been analyzed for major dissolved components. Cations and anions were analyzed by conventional Inducted Coupled Plasma with Atomic Emission Spectrometry (ICP-AES) and High Performance Liquid Cromatrography (HPLC), respectively, with an standard error lower than 5% in all cases. The δD and $\delta^{18}O$ values for the same two water samples were determined by H_2 and CO_2 equilibrium respectively and Isotope Ratio Mass Spectrometry (IRMS). The data were reported in the usual $\delta^{18}O$ and δD SMOW. The sample from level 530 has been also analyzed for tritium counting with a precision of ±0.31 TU (1 TU = 10^{-18} $^3H/^1H$). These data are summarized in Table DR4.

Table DR4: Chemical analyses (mg/L) of water samples from Naica mine. Legend : 290-1976, means sample collected at level 290 m in 1976. * (asterisk), measured at 20°C. Analyses 290-1976 and 430-1976 are after Dames and More (1977). The saturation index of some main minerals has been calculated with the code PHREEQC (Parkhusrt and Appelo, 2003).

	290-1976	**390-1976**	**430-1976**	**640-2002**	**530-2003**
Temperature (°C)	54	53	54	52	53
pH *	7.2	7.4	7.4	7.2	7.1
Alkalinity ($CaCO_3$)*	160	170	170	130	100
Cl (mg/L)	24	21	21	22	28
SO_4	2130	1960	2140	1922	2033
F	2.5	2.6	2.1	2.8	2.5
Ca	640	660	690	585	643
Mg	130	120	110	124	121
Sr	4.5	3.9	3.9	11	11.4
Na	120	125	110	89	96
K	11	11	11	14	13
SiO_2	75	110	50	33	31
Al	1.1	2.3	2.3	<0.1	<0.1
Mn	0.22	0.27	0.26	0.02	0.03
Fe	2.5	0.82	0.7	<0.1	<0.1
$\delta^{18}O$ (per mil)	-7.5	-	-7.8	-7.8	-7.5
$\delta^{2}H$ (per mil)	-58.7	-	-56.9	-57.0	-57.5
^{3}H (UT)	-	-	-	-	<0.31
Saturation Index					
Calcite	0.41	0.64	0.68	0.28	0.10
Dolomite	0.54	0.94	0.96	0.31	-0.11
Anhydrite	-0.01	-0.04	0.02	-0.09	-0.03
Gypsum	0.02	0.01	0.05	-0.03	0.01
Fluorite	-0.13	-0.06	-0.24	-0.02	-0.11
Chalcedony	0.35	0.52	0.17	0.01	-0.03
Celestite	-0.35	-0.44	-0.42	0.02	0.02

3. Supplementary Discussion

3.2 Gypsum Nucleation

Solubility curves for gypsum and anhydrite as a function of temperature and salinity have been computed using version 2.12.1-669 (Linux) of the PREEQC software of the U.S. Geological Survey for three different pH values (6.0, 7.0 and 8.0) and three different salinity values. Calculations identified as "salinity 1" included a concentration of Na, Cl and Mg equal to the one measured in present-day waters collected in the Naica mine (100 mg/L Na, 24 mg/L Cl and 120 mg/L Mg). "salinity 2" conditions include twice this concentration and, finally, "salinity 0" calculations were made starting with pure water. In contrast with the negligible effect of pH, the salinity is a major control in the solubility of both gypsum and anhydrite. Fig. 4a of the paper shows these solubility curves.

Supersaturation values were calculated as $\sigma(T) = m_a(T)/m_g(T)$ where m_a and m_g are the equilibrium concentration of Ca in a saturated solution in equilibrium at temperature T with anhydrite and gypsum respectively as calculated by PHREEQC. This means that $\sigma(T)$ is the supersaturation with respect to gypsum of a solution obtained by equilibrium dissolution of anhydrite at temperature T. The computed supersaturation values as a function of T are shown in figure DR10.

The curves of induction time for nucleation were in turn computed from these supersaturation curves using equation

$$J = A\exp - \frac{16\,\pi\gamma^3 v^2}{3\mathrm{k}^3 T^3 ln^2 S}$$

discussed in the article. Data from three different papers have been analyzed to collect the empirical data to parameterize this equation (Lancia *et al*., 1999; Prisciandaro *et al.*, 2001; He *et al.,* 1994). These articles show a considerable scattering in the values of activation energy, which is a critical parameter for the nucleation and can have a very large impact (several orders of magnitude) in the value of the induction time. Fortunately, owing to the extremely step slope of the induction time curve, these changes can only produce shifts of a few degrees in temperature for reasonable time values in the range "one day" to "some thousand of years". Consequently, the inherent uncertainty in these empiric data does not compromise our results and the only expected influence is a shift of (at most) 5 ºC in the lower boundary of the temperature window proposed. The parameters used for the curves shown in the article (Fig. 4b) were obtained from Lancia *et al*. (1999) because this article contains data for supersaturation values smaller than the remaining references, making more accurate the extrapolation needed for the very low supersaturation values involved in the crystallization of the Naica gypsum crystals.

3.3 Evidence of phase transition anhydrite-gypsum in Naica

Several mineral samples of gypsum, anhydrite and enclosing limestone were collected from the Caves of Crystals, Swords and Queen and from the surroundings. The mineralogy of the samples was investigated by transmitted light microscopy, Powder X-ray diffraction method (XRD), and by Scanning Electron Microscopy and microanalysis (SEM-EDS). In Figure DR11 evidence of a transformation anhydrite-gypsum at microscopic level is shown.

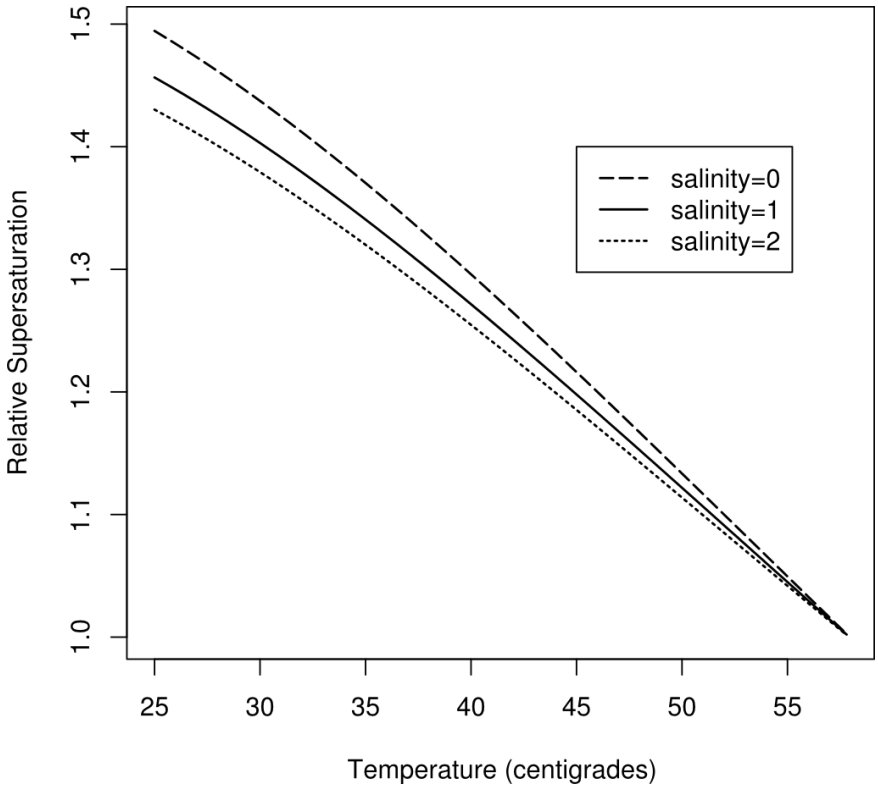

Figure DR10: Temperature dependence of supersaturation with respect to gypsum of a solution obtained by equilibrium dissolution of anhydrite.

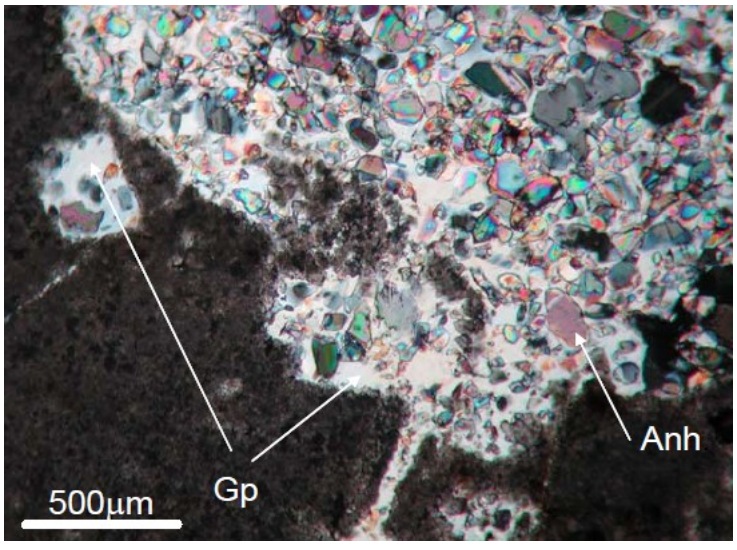

Figure DR11: Poikiloblastic gypsum crystals growing inside an anhydrite matrix. Sample collected close to the Cave of Crystals, Naica mine, level 290.

4. References cited in the supplementary materials

Bakker, R. J., 2003, Package FLUIDS 1. Computer programs for analysis of fluid inclusion data and for modeling bulk fluid properties: Chemical Geology, v. 194, p. 3-23.

Bodnar, R. J., 1993, Revised equation and table for determining the freezing point depression of H_2O-NaCl solutions. Geochimica Cosmochimica Acta, v. 57, p. 683-684.

Butler, G.P., 1973, Strontium geochemistry of modern and ancient calcium sulphate minerals, in Purser, B.H., ed., The Persian Gulf: Springer-Verlag, Berlin Heidelberg New York, p. 423-452.

Dames and More, 1977, Reporte de Estudio hidrogeológico de Naica. Compañía Fresnillo S.A. de C.V. Internal report.

Degoutin, N., 1912, Les grottes a cristaux de gypse de Naica (Mexique): Soc. Cient. Ant. Alz. Rev. 32, 35-38.

Foshag, W., 1927, The Selenite Caves of Naica, Mexico: American Mineralogist, v. 12, p. 252-256.

He, S., Oddo, J. E. and Tomson. M. B., 1994, The nucleation kinetics of calcium sulphate dehydrate in NaCl solutions up to 6 m and 90 ºC: Journal of Colloid Interface Science, v. 162, p. 297-303.

Lancia, A., Musmarra, D. and Prisciandaro, M., 1999, Measuring Induction Period for Calcium Sulfate Dihydrate Precipitation: AIChE Journal 45, 390-397.

Parkhurst D. L. and Appelo C.A.J., 2003, PHREEQC- A hydrogeochemical transport model. http://wwwbrr.cr.usgs.gov/projects/GWC_coupled/phreeqc/index.html

Pearson F.J. Jr. and Rightmire, C.T., 1980, Sulphur and oxygen isotopes in aqueous sulphur compounds., in Fritz, P. and Fontes, J. Ch. (Eds.), Handbook of Environmental Isotope Geochemistry. Elsevier.

Prisciandaro, M., Lancia, A., and Musmarra, D., 2001, Gypsum nucleation into sodium chloride solutions: AIChE Journal, v. 47, 929-934.

Simon, B., and Bienfait, M., 1965, Structure et mécanisme de croissance du gypse: Acta Crystallographica, v. 19, p. 750-756.

Thode H.G., and Monster, J., 1965, in Fluids in Subsurface Environment, AAPG Memoir nº4. 367-377.

5. Acknowledgments for supplementary materials

We acknowledge María del Carmen Jimenez de Haro (Instituto de Ciencia de Materiales de Sevilla) for operation of the scanning electron microscope.